Mechatronic Design and Positioning Accuracy Characterisation of a Robotic Arm for Exploration Rovers

Giacomo Franchini
School of Engineering
University of Padova
Padova, Italy
giacomo.franchini.1@studenti.unipd.it

Sebastiano Chiodini
Dept. of Industrial Engineering
University of Padova
Padova, Italy
sebastiano.chiodini@unipd.it

Marco Ghetti
School of Engineering
University of Padova
Padova, Italy
marco.ghetti@studenti.unipd.it

Marco Pertile
Dept. of Industrial Engineering
University of Padova
Padova, Italy
marco.pertile@unipd.it

***Abstract*—Upcoming planetary exploration missions will see extensive use of rovers for both scientific tasks, building tasks and astronaut assisting tasks. An essential element to carry out these tasks is the presence of a robotic arm. In this work, the mechatronic design of a lightweight and modular robotic arm for a planetary exploration rover is presented. The presented 4DOF solution was found to provide enough dexterity to collect target samples due to the non-holonomic constraints provided by the arm's supporting rover, allowing reduced mass and power budget. The rover arm control software is based on the Robot Operative System (ROS) framework. Positioning accuracy has been evaluated with TagSLAM, a low-cost tracking method based on AprilTag fiducial markers.**

***Index Terms*—Robotic Arm, Rover, AprilTag, Pose Estimation, ROS**

I. Introduction

Robotic planetary exploration has seen a wide use of rovers in different mission scenarios, involving a variety of profoundly different tasks from each other. In order to reach a site of scientific interest, rovers must be able to traverse rough terrains, planning safe paths and avoiding obstacles. At the same time, the robots need to localize themselves in an unstructured environment while generating and storing a map of it. Once on site, the ability of correctly deploy an instrument and to perform ground sample analysis for scientific investigation is needed [1]. An essential element to perform these tasks is a robotic arm assembled on the robot [2]. Planned missions foreseen the deployment of scientific stations, such as the LightWeight Rover Unit concept [3], and sample retrieval and collection, as for the Mars Sample and Return (MSR) mission [4]. In future missions, building and assisting tasks will be implemented, and rovers will be able to provide support for human exploration and infrastructure construction. International competitions such as the University Rover Challenge and the European Rover Challenge have led to the development of planetary rover testbeds by university teams [5]. [6] presents the development of a 6 DOF manipulator for a rover testbed targeted at these kinds of competitions.

At the University of Padova, the MORPHEUS (Mars Operative Rover of Padova Engineering University Students) educational rover has been developed as a support for Space Robotics courses and as a testbed for robotic exploration technologies. It was designed considering the main constraints typical of space systems, even if space-qualified components were avoided to favor rapid prototyping. The rover prototype presents a six-wheel skid steering configuration, and its control system is based on the ROS (Robot Operating System) framework [7]. The rover is capable of autonomous navigation thanks to a visual subsystem in which a stereo camera and LiDAR operate together in a sensor-fusion approach [8].

On such bases, we developed a lightweight robotic arm targeted to the Martian missions. In particular, the arm is designed for multi-purpose lander/rover applications like: (1) acquisition of a cached sample, as in the case of the Sample Fetching Rover for Mars Sample Return [9], (2) scientific instrument deployment from lander [3], (3) sample collection and deposition by equipping the robotic arm with a scoop/blades that enable sample collection from the planetary surface, as was the case for the Phoenix [10] and InSight missions [11]. In both the case of scientific instrument deployment from the lander and sample collection and deposition with scoop/blades a robotic arm with 4 DOF is sufficient.

This work has been supported by Progetti Innovativi degli Studenti, University of Padova, and Progetti Studenteschi a Carattere Competitivo e non, Department of Industrial Engineering - University of Padova. We would like to thank the Morpheus Team for the discussions and participation in the experiments.

The reasons will be explained in point B. Kinematic Structure in Section II. It is preferable to use contactless measurement methods to describe or define the precision of the positioning of the end-effector. Very often, to do this, the end effector is equipped with retro-reflective spheres, which are then traced by means of a laser tracker with an accuracy better than 0.1 mm [12], or by motion capture system with millimetric accuracy. However, if positioning requirements are less stringent, vision systems can also be used, since are less expensive and easier to set up. For example in [13], the authors present an experimental setup for measure the end effector position, in which a camera is used to detect a LEDs pattern installed on the manipulator. In this work, we used a pose estimation method based on AprilTag fiducial markers [14].

The main contributions of this work to the current literature are twofold: first, we present the work done for designing and testing a modular four degree-of-freedom robotic arm interfaced with ROS, that will be integrated with the aforementioned rover. Second, we evaluate positioning accuracy with a low-cost tracking system based on fiducial markers.

In Section II we analyze the kinematic model defined for the manipulator. Based on this configuration, the manipulator workspace is illustrated. Section III describes the mechanical design of the robot. Section IV is dedicated to robotic arm gearmotor control. Then the ROS integration of the manipulator is presented for the connection within the control system of the rover. To achieve this, we created a ROS workspace that contains packages for motor and gripper driver connection and manipulator forward/inverse kinematic, allowing robotic arm control. Lastly, in Section V, the accuracy and repeatability of the system have been characterized in terms of the end effector position and orientation inside the workspace, in order to verify the compliance of the system with the design requirements. In Section VI the concluding remarks are reported.

II. Kinematic Analysis

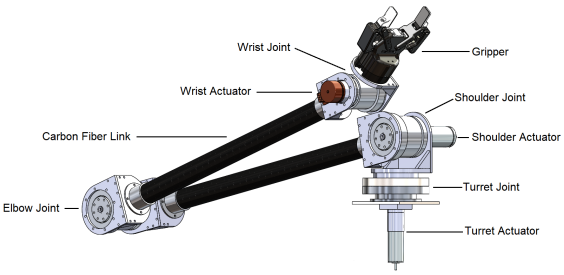

Fig. 1: Robotic arm layout.

A. Design Requirements

The primary functional requirement of the proposed robotic arm is the ability to position its end effector, a 1 kg gripper, at any point within the workspace with a desired pose while respecting all performance requirements and constraints imposed on the system. Moreover, in order to pursue mission objectives in an appropriate manner, the robotic system must satisfy a series of performance requirements. Their definition is of fundamental importance as it will influence all choices to be made during the manipulator design process: the kinematic configuration, the gearmotors at the joints, the type of end effector, and the power and control system. The key performance requirement is the repeatability of the end effector's position. Targeting the collection of spherical or cylindrical rocks and objects, and using off-the-shelf grippers, with a typical stroke of 85 mm, the object's center of gravity must be contained within the stroke, therefore, we consider a maximum placement error (lateral position error) of ± 43 mm. The repeatability shall be less than ± 15 mm.

B. Kinematic Structure

It is clear that the greater the number of degrees of freedom of the system, the greater its dexterity is. A robot with 6 degrees of freedom is able to position the end effector at any point within its workspace with the desired pose. Additional degrees of freedom makes the robot redundant, increasing its versatility of movement. On the other hand, more DOF correspond to an higher mass and system complexity, due to the additional actuators, sensors, and components. Considering the type of target (spherical rock samples and cylindrical sample tubes), and that the rover that will house the arm operates in mostly flat terrain, it was considered sufficient to use a 4 DOF system of the yaw-pitch-pitch-pitch type, as shown in Fig. 4d in D. Use Case Example section. The first joint is positioned at the base and allows rotation around the yaw axis, whereas the three subsequent joints allow rotation around the pitch axis. The configuration of the robotic arm is shown in Fig. 1. Fig.2 shows the kinematic configuration chosen.

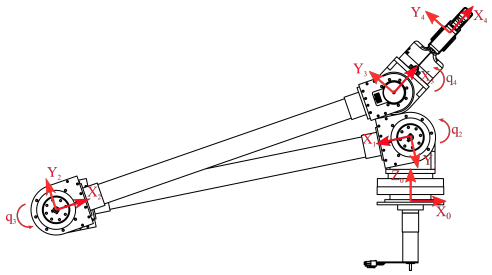

Fig. 2: Kinematic configuration chosen for the robotic arm.

C. Workspace

The manipulator workspace has been defined as a square-cuboid with $800 \times 500 \times 500$ mm sides positioned in front of the rover. Reachability requirements are met thanks to the dimensions of the two main links, numbers 2 and 3, both of which are 570 mm long. The end effector reference system was positioned a further 100 mm away from the previous one. From the base to the gripper interface plate, the arm is 1240 mm long.

D. Use case example

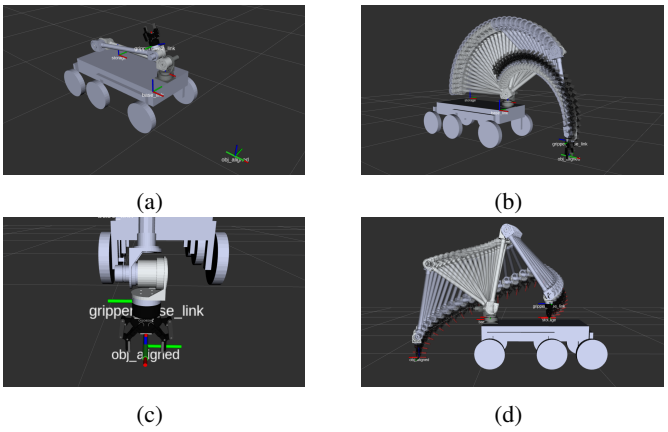

Fig. 3: Simulation of sample collection by means of the robotic arm on the carrier rover showed in the 3D visualizer for the ROS framework Rviz, simulations performed considering a Robotiq 2F-85 gripper. Sample axis aligned with the gripper axis case study: (a) sample approach, (b) end effector positioning, (c) sample collection and (d) sample transfer to the sample bin.

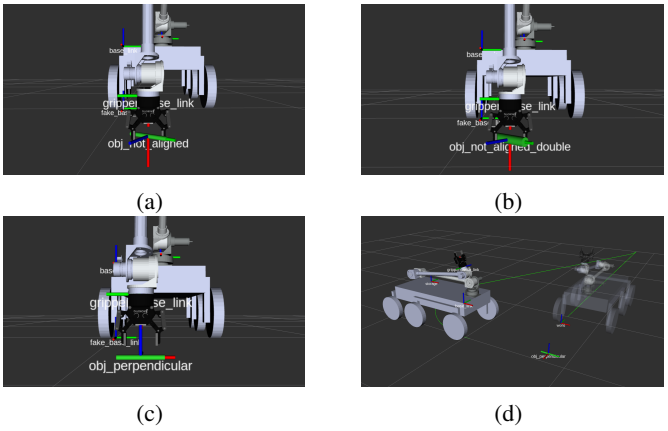

Fig. 4: Sample collection simulation in the case of misalignment between the axis of the sample and the axis of the gripper, simulations performed considering a Robotiq 2F-85 gripper. (a) 15 mm sample tube diameter: collection is possible up to a misalignment of 66°. (b) 30 mm sample tube diameter: collection is possible up to a misalignment of 56°. (c) In case of axes perpendicularity sample collection is not possible, however, the rover can be repositioned in order to align the axes (d).

The collection of samples has been analyzed using the robotic arm installed in the carrier rover system. Simulations have been performed in Rviz. In particular, a sample placed on a flat surface was analyzed. In Fig. 3 it is possible to see the simulation results if the sample axis is aligned with the gripper axis: the rover approaches the sample (Fig. 3a), the end effector is positioned over the sample within the gripper stroke (Fig. 3b), the gripper is tightened on the sample (Fig. 3c) which is then transferred to the sample bin on the rover (Fig. 3c).

If the gripper has a stroke larger than the diameter of the sample, the sample could also be taken if there is a misalignment between the sample's axis and the gripper's axis, as shown in Fig. 4. Fig. 4a shows the simulations performed with a Robotiq 2F-85 gripper to collect a 15 mm sample tube diameter, the allowable misalignment is 66°. Instead the Fig. 4b shows the case of a 30 mm sample tube, where the allowable misalignment is 56°. However, thanks to the non-holonomic constraint provided by the rover, the proposed 4DOF robotic arm provides sufficient dexterity to collect the sample if a rover-to-sample alignment maneuver is performed, as shown in Fig. 4d.

III. Mechanical Design

A. Gearmotor Selection

The kinematic model of the robotic arm was used to create a Simulink model on which simulations are carried out. The simulation results were used within an iterative process, which allowed the selection of gearmotors. Over the multiple simulations carried out for the actuator choice, the torques obtained from a maneuver in which the manipulator rotates for 90 degrees about the joint 2 axis, while completely extended, have been considered. Such a conservative choice has been followed to make the robot able to follow any trajectories in its workspace and to allow overload, as the maneuver is the one which requires higher motor effort. The greatest torque is expected at Joints 2 and 3, where we find a torque of 45 Nm and 15 Nm respectively. The gearmotors for joint 1, 2 and 3 belong to Maxon EC-i series. For joint 4, a different type of motor was chosen, from the Maxon EC-flat series, in order to favor the axial compactness of the joint assembly while respecting the functional requirements.

B. Joint and link design

For the mechanical design of the joints of the Morpheus rover manipulator, we started from the overall dimensions of the motor-reducer assemblies identified in Section III-A. This is because an attempt has been made to create a joint design that allows the gearmotors to be integrated internally, in such a way as to reduce the axial dimensions and, therefore, the cantilever loads on the system. All custom components were made of aluminum-silicon-magnesium-manganese alloy AA6082. 6000 alloys have a good compromise between mechanical strength and density, offering corrosion resistance and excellent machinability. The overall mass of the robotic arm, excluding the gripper, is 9.65 kg. Joint 1 is shown in Fig. 5. Joints 2 and 3 are shown in Fig. 6. Joint 4 is shown in Fig. 7

Connections to the links are made by means of L-shape elements, made by joining two plates, which have a series of holes for connection and two reinforcing ribs. Joint number 2 is connected directly to the driven flange of joint number 1, creating a compact design at the base of the robot. Between joints 2, 3, and 4, there are two main links of the manipulator,

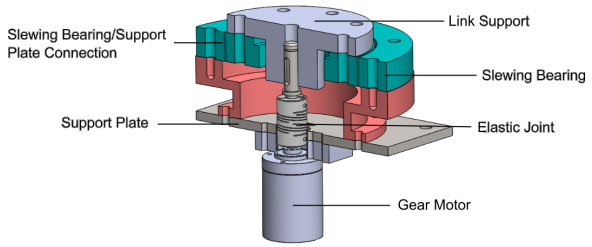

Fig. 5: Internal view of the turret joint (Joint 1).

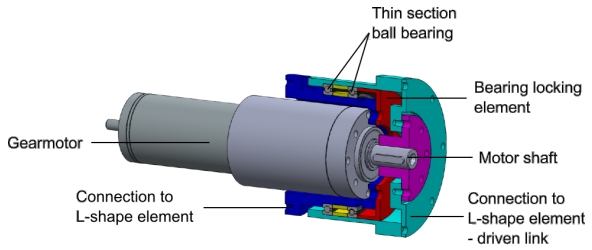

Fig. 6: Internal view of the shoulder and elbow joint (Joints 2 and 3)

made with a tubular carbon fiber Carbosix, with a diameter of 40 mm, thickness 1.5 mm and length 570 mm each. Two perforated aluminum flanges were glued to the head and tail of the tubulars to connect to the joints using L-shaped elements. Scotch-Weld 3M 490 epoxy resin has been used as bonding element.

1) End effector selection: The end effector selected for sample collection is the Robotiq 2F-85 Adaptive gripper, which has a stroke of 85 mm. The gripper is equipped with two fingers made using articulated quadrilaterals, each formed by two phalanges, whose movement is carried out using a single actuator. The configuration described allows the gripper to adapt to the shape of the object to be grasped, ensuring up to five points of contact, four of which with the phalanges and one with the palm. The gripper is equipped with a separate base, which allows for 24 V power supply and data transfer, as well as installation on the robotic arm using 4×M6 screws. The gripper, which is shown in Fig. 8, is connected to the

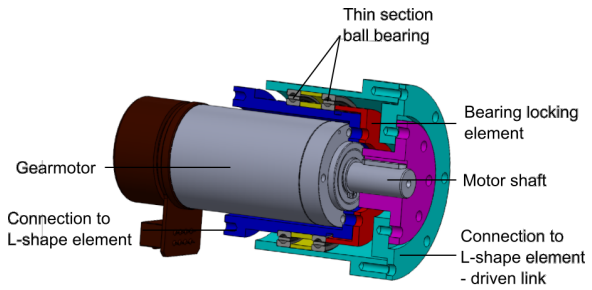

Fig. 7: Internal view of the wrist joint (Joint 4).

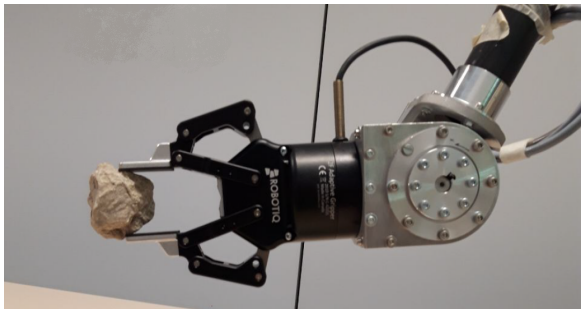

Fig. 8: The end effector assembled on the robotic arm.

output plate operated by joint 4.

IV. Arm Control

The selected motor drivers are the Maxon EPOS4 CAN Compact 50/8 board for the joints 2, 3, and 4 motors, and the Maxon EPOS4 CAN Compact 50/5 board for the joint 1 motor. The drivers are connected to the workstation via USB protocol. The encoders assembled in the gearmotors have 3 channels, two of which, A and B, determine the rotation of the motor and the direction of motion, clockwise or counterclockwise, while a third determines the position of 0. The encoders are characterized by 1024 step-per-turn resolution and Gray code is used for decoding the signal.

Sinusoidal commutation has been chosen for motor current switching. In this case, switching is achieved by applying a current with a sinusoidal trend to the windings, depending on the information on the angular position of the rotor. This method ensures low torque ripple by minimizing the noise generated by the motor, but requires the presence of an additional sensor for the accurate measurement of the motor rotation. The EPOS4 board regulator architecture foresees three different loops integrated within it: a current regulator, used in any operating mode, a position regulator and a speed regulator, used, respectively, in the operating modes based on position and speed.

V. Test and Results

In this section, the results of the test campaign are shown. The accuracy and repeatability of the system have been characterized in terms of positioning and orientation of the end effector in the workspace. Both characteristics contribute to the difference between the controlled pose and the pose actually achieved. To characterize both the accuracy and the repeatability of the system, the end effector must reach a set of waypoints one after the other. The choice of points is in accordance with the ISO 9283: 1998 standard, which governs the criteria for classifying the performance of manipulators and test methods. A parallelepiped portion of the working space is then chosen, with the faces parallel to the axes of the fixed reference system at the base of the robot. A diagonal plane is then defined within the volume of the parallelepiped, called the measurement plane. Fig. 9 displays the selected measurement points, namely P1, P2, P3, P4, and P5, which are located on

TABLE I: End effector controlled poses (x, y, z, θ) for the various measuring points. Systematic errors (total error e_{tot} and its components e_X, e_Y, e_Z, lateral positioning error e_{EF}, and angular error e_θ) and repeatability (σ_l and σ_θ) to reach the target pose.

Point	**X** [m]	**Y** [m]	**Z** [m]	θ [rad]	e_{tot} [m]	e_{EF} [m]	e_X [m]	e_Y [m]	e_Z [m]	σ_l [m]	e_θ [rad]	σ_θ [rad]
P1	0.3	-0.076	0.4	0.5	0.029	0.023	0.022	0.007	0.017	0.011	0.002	0.005
P2	0.5	0.3	0.6	0.5	0.046	0.038	0.009	0.043	0.013	0.005	0.061	0.004
P3	0.5	-0.3	0.6	0.5	0.050	0.042	0.001	0.049	0.009	0.005	0.010	0.004
P4	0.2	-0.3	0.2	1	0.036	0.020	0.024	0.027	0.001	0.007	0.013	0.006
P5	0.2	0.3	0.2	1	0.046	0.026	0.036	0.029	0.002	0.007	0.020	0.005

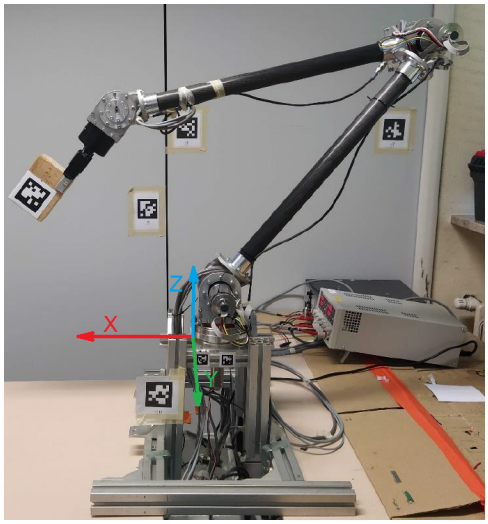

Fig. 9: Experimental setup dedicated to the position accuracy and repeatability of the robotic arm.

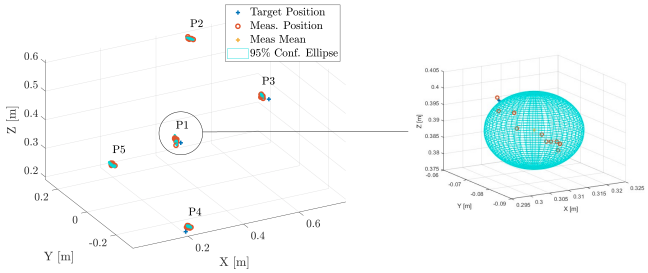

Fig. 10: Comparison between target position (obtained through encoder feedback) and repeated measurements performed through TagSLAM tracking with their 95% confidence ellipse.

the two diagonals of the measuring plane. To evaluate the repeatability, the robot is made to reach the five points in succession 10 times, the measurement points coordinates are reported in Table I.

To estimate the pose of the end effector, two series of different measurements were carried out, one using an external sensor (a camera) and one made using internal sensors (the gearmotor encoders). The TagSLAM package [14] was used to reconstruct the end effector pose from the camera-based measurements. TagSLAM allows object pose estimation to be implemented in a flexible and robust way, using AprilTag fiducial markers [15]. Reconstruction of the pose using AprilTags showed a positioning accuracy better than one centimeter for a target placed less than 1 m away and a rotational accuracy better than 0.5 degrees [16]. The use of fiducial markers showed even better performances in the reconstruction of spacecraft poses [17], making it an adequate tool for the type of characterization to be carried out. During the tests carried out on the manipulator, tags of the 36h11 family were used.

The experimental setup is shown in Fig.9.

A. *Results*

The collected data were used to determine the accuracy and repeatability of the system, in terms of positioning and orientation of the end effector in the workspace. The systematic error of the end effector positioning has been defined as the difference between the input pose position (obtained from feedback from the encoders) and the center positions measured by means of AprilTags tracking, used as reference. The orientation accuracy of the end effector has been defined as the difference between the orientation of the input pose (obtained from feedback from the encoders) and the average of the orientations actually measured by AprilTags tracking. The lateral position error e_{EF} is given by the planar components of the error along the gripper stroke $e_{EF} = e_{XY} \cos\theta$ where θ is the angle that the plane of movement of the arm forms with the XY plane and $e_{XY} = \sqrt{(\bar{X} - X_{in})^2 + (\bar{Y} - Y_{in})^2}$ is the planar error.

Figure 10 shows the results obtained in terms of systematic error and repeatability. The target position to be reached is represented by a blue cross, while the values obtained from the camera measurements are indicated by a red circle. The straight line connects the target position to the center of gravity of the measurements made and provides a visual representation of the systematic error of the system. The 95% confidence ellipsoids show the repeatability of the system positioning; it is centered in the barycenter of the measurements. The accuracy of the system is determined by the contribution of the systematic errors present during the execution of the measurements, which involve the presence of an offset between the measured and the commanded configurations, and by the contribution of

the repeatability of the system.

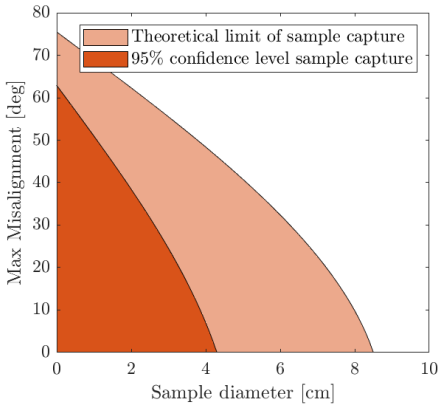

Fig. 11: Maximum misalignment between the sample axis and the capture gripper for different sample sizes to capture without needing to run a rover repositioning maneuver.

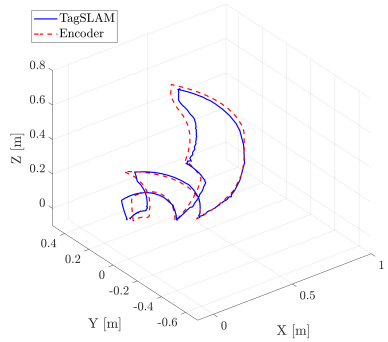

Fig. 12: Comparison between the trajectory measured by the motor encoders and the position detected by AprilTags tracking.

In Table I the results obtained from the camera measurements are listed for each measurement point. Total positioning and orientation accuracy are, respectively, 0.050 m and 0.061 rad (around 3.5°). The lateral positioning accuracy is better than 0.042 m and the repeatability is better than 0.011 m, thus meeting the performance requirements, as stated in Design Requirements in Section II. Fig. 11 illustrates the maximum size of objects that can be grasped without a rover repositioning maneuver, as well as the maximum possible misalignment between the sample axis and the Robotiq 2F-85 gripper axis for different sample sizes. The figure also shows the theoretical limit and the limit considering the arm positioning accuracy (95% confidence). Additionally, the figure displays the maximum size of targeted objects that can be grasped, taking into account their misalignment relative to the gripper axis and the gripper positioning repeatability. Fig. 12 shows the comparison between the trajectory measured by the motor encoders and the position detected via AprilTags tracking. Trajectory tracking in the example shown in the figure gives an average positioning error of 0.047 m.

VI. Conclusions

This paper illustrates the work carried out to design and build a modular 4 DOF robotic arm interfaced with ROS targeted to planetary rover exploration. We showed that due to the non-holonomic constraints provided by the rover that houses the robotic arm and given that most of the cached samples are at ground level, the 4 DOF solution offers sufficient dexterity to collect samples at reduced mass and power budget. The final design of the robotic arm and its joints is presented. The positioning accuracy of the end effector was evaluated in a laboratory environment. Fiducial markers and the TagSLAM trajectory reconstruction method were used as the measurement method. The total positioning and orientation accuracy are, respectively, 0.050 m and 0.061 rad. The accuracy of lateral positioning is better than 0.042 m and the repeatability is better than 0.011 m, thus meeting the performance requirements.

References

[1] R. C. Anderson *et al.*, "Collecting samples in gale crater, mars; an overview of the mars science laboratory sample acquisition, sample processing and handling system," *Space science reviews*, vol. 170, no. 1-4, pp. 57–75, 2012.

[2] P. S. Schenker *et al.*, "Planetary rover developments supporting mars exploration, sample return and future human-robotic colonization," *Autonomous Robots*, vol. 14, no. 2, pp. 103–126, 2003.

[3] P. Lehner *et al.*, "Mobile manipulation for planetary exploration," in *2018 IEEE Aerospace Conference*. IEEE, 2018, pp. 1–11.

[4] B. K. Muirhead *et al.*, "Mars sample return campaign concept status," *Acta Astronautica*, vol. 176, pp. 131–138, 2020.

[5] M. Post and R. Lee, "Lessons learned from the york university rover team (yurt) at the university rover challenge 2008–2009," *Acta Astronautica*, vol. 68, no. 7-8, pp. 1343–1352, 2011.

[6] L. Sohlbach *et al.*, "Development of a 6 dof manipulator for a mobile robot," in *2021 International Conference on Advanced Mechatronic Systems (ICAMechS)*. IEEE, 2021, pp. 121–124.

[7] S. Chiodini *et al.*, "Design of a user-friendly control system for planetary rovers with cps feature," in *2021 IEEE 8th International Workshop on Metrology for AeroSpace (MetroAeroSpace)*. IEEE, 2021, pp. 317–321.

[8] S. Chiodini *et al.*, "Retrieving scale on monocular visual odometry using low-resolution range sensors," *IEEE Transactions on Instrumentation and Measurement*, vol. 69, no. 8, pp. 5875–5889, 2020.

[9] A. Merlo *et al.*, "Sample fetching rover (sfr) for msr," in *Proceedings of the 12th Symposium on Advanced Space Technologies in Robotics and Automation (ASTRA 2013)*, 2013.

[10] R. Bonitz *et al.*, "The phoenix mars lander robotic arm," in *2009 IEEE Aerospace conference*. IEEE, 2009, pp. 1–12.

[11] A. Trebi-Ollennu *et al.*, "Insight mars lander robotics instrument deployment system," *Space Science Reviews*, vol. 214, no. 5, pp. 1–18, 2018.

[12] S. Kyle *et al.*, "Robot calibration by optical methods," in *IEE Colloquium on Next Steps for Industrial Robotics*. IET, 1994, pp. 9–1.

[13] A. Caon *et al.*, "Development and test of a robotic arm for experiments on close proximity operations," *Acta Astronautica*, vol. 195, pp. 287–294, 2022.

[14] B. Pfrommer and K. Daniilidis, "Tagslam: Robust slam with fiducial markers," *arXiv preprint arXiv:1910.00679*, 2019.

[15] E. Olson, "Apriltag: A robust and flexible visual fiducial system," in *2011 IEEE International Conference on Robotics and Automation*, 2011, pp. 3400–3407.

[16] M. Kalaitzakis *et al.*, "Fiducial markers for pose estimation," *Journal of Intelligent & Robotic Systems*, vol. 101, no. 4, pp. 1–26, 2021.

[17] M. Pertile *et al.*, "Metrological characterization of a vision-based system for relative pose measurements with fiducial marker mapping for spacecrafts," *Robotics*, vol. 7, no. 3, p. 43, 2018.